ROYAL SOCIETY OF CHEMISTRY

PAPER

Check for updates

Effect of polyacrylamide gel elasticity on collagen type II fibril assembly†

Kathryn G. Wilcox, [a] Stephanie Kramer, [b] Surajit Chatterjee, [b] Adam Linscott, [a] Sneha Suresh, [a] Lydia Kisley [bc] and Svetlana Morozova ⋆[a]

Collagen type II fibrils provide structural integrity to the articular cartilage extracellular matrix. However, the conditions that control the fibril radial size scale, distribution, and formation inside of dense networks are not well understood. We have investigated how surrounding elastic networks affect fibril formation by observing the structure and dynamics of collagen type II in model polyacrylamide gels of varying moduli. Cryogenic transmission electron microscopy (cryo-TEM) is used to image the fibril structure and is verified qualitatively with optical microscopy of fluorescently-tagged collagen within the gels. Using fluorescence correlation spectroscopy super-resolution optical fluctuation imaging (fcsSOFI), the diffusion dynamics of the collagen in low pH and neutral pH conditions are determined. Overall, the fibril bundle diameter and concentration were found to decrease as a function of gel modulus. The single fibril diameter remains constant at 30 nm within the gels; however, the diameter was found to be smaller when compared to in solution. Additionally, the mode of diffusion of the collagen triple helices changes within gel environments, decreasing the diffusion coefficient. Understanding the intricate relationship between network topology and collagen type II fibril formation is crucial in gaining deeper insights into the transport phenomena within complex acellular tissues that are necessary for the development of future therapeutic materials.

Introduction

Collagen type II is a critical protein that gives structural integrity to the extracellular matrix (ECM) of articular cartilage and is one of six types of collagen that self-assembles into fibrils.[1] The protein is a homotrimer with a distinct glycine–X–Y motif where X and Y are most commonly proline and hydroxyproline.[2,3] Electrostatics and hydrophobic interactions are largely thought to drive fibril formation, but these interactions alone do not explain the equilibrium radial length scales of the assembly.[4] Previous studies from Grason and Bruinsma,[5] Grason,[6] Morozova *et al.*,[4] and Wilcox *et al.*[7] have found a possible relationship between the fibril radius and the persistence length, a measure of intrinsic elasticity. However, these studies all take place in solution, whereas collagen typically forms fibrils in the dense network environments of the articular cartilage ECM where fibril radius can depend on local protein and carbohydrate concentration. Collagen type II is a large protein with a contour length of

~300 nm, which limits the current understanding of the diffusion and self-assembly mechanisms in tight, complex networks like the ECM.

In the articular cartilage ECM, collagen fibrils are hierarchically organized in hyaluronic acid (HA) and proteoglycan gels.[2,8,9] Individual fibrils are typically distinguished by characteristic striations along the fibril, called D-banding, and often aggregate into larger structures called bundles. These gels have a high osmotic modulus that resists compressive loads due to their polyelectrolyte nature.[8,10–12] Collagen fibrils increase the overall mechanical properties such as the gel modulus.[13,14] The mesh size and the internal pressure of the gels also have the capacity to greatly influence collagen structure. For example, the correlation between fibril structure and the local gel concentration is frequently discussed in literature.[9] Lane and Weiss describe that collagen fibril diameter increases with articular cartilage depth.[9] Giraud-Guille *et al.*[15] and Salameh *et al.*[16] have also shown that collagen organization depends on the concentration if the concentration is high enough. Moreover, ECM tissues such as articular cartilage are avascular and mostly acellular, which limits the ability to self-repair. Chondrocytes, the cells responsible for making new collagen, account for only 1–3% of the entire matrix, and some healing mechanisms involve the deposition and diffusion of collagen through the matrix. Diffusion through the ECM is known to be complicated by the network density which creates

a Department of Macromolecular Science and Engineering, Case Western Reserve University, Cleveland, OH, USA. E-mail: svetlana.morozova@case.edu

b Department of Physics, Case Western Reserve University, Cleveland, OH, USA

c Department of Chemistry, Case Western Reserve University, Cleveland, OH, USA

† Electronic supplementary information (ESI) available: Optical microscopy videos and additional gel characterization data. See DOI: https://doi.org/10.1039/d4sm01104j

barriers to mobility and can impact transport due to chemical interactions.[17] The available volume and connectedness of the extracellular environment in phantom tissues has been studied to understand the role of the matrix density on tumor growth and drug delivery.[18,19] Network interactions have also been shown to selectively filter macromolecules based on charge and size, indicating the complexity of transport within these tissues.[20]

Diffusion of macromolecules through elastic networks is complex even within model systems. Often, transport and motion are characterized by several regimes depending on the topology of the network and the particle size relative to the network mesh size. Gels, including biological tissues, are often inhomogeneous and include topological constrains that can impact diffusion.[21] Heterogeneous structure with regions of high and low crosslink densities can develop due to chain overlap at crosslinking, monomer and crosslinker reaction kinetics, frozen-in concentration fluctuations, and microsyneresis during gelation.[22,23] With increasing crosslink percent, more heterogeneities occur.[24] For polyacrylamide gels, there is a critical gel concentration where the degree of heterogeneities reaches a maximum in relation to the initial monomer concentration.[25] Above 7% crosslinking, the modulus starts decreasing with increasing crosslinking as a result of gel topology. There are length scales that are associated with inhomogeneities of networks. The average distance between crosslinks is referred to as the mesh size of the gel, ξ, and, often, there are larger length scales associated with areas of lower crosslink density, of average size d_p. While ξ for polyacrylamide gels is on the order of 10 s of nanometers, d_p has been estimated to be ~100–150 nm from particle tracking experiments.[26]

Increases in crosslinking correlate to increases in heterogeneity, smaller mesh sizes, and stiffer networks that change diffusion within the gel. Softer gels have much larger mesh sizes, which allow for small particles to diffuse more freely on shorter time scales. As the particle size approaches the gel mesh size, there is greater confinement which leads to trapping.[27,28] This leads to different diffusion regimes depending on the size of the diffusing particle or macromolecule and the gel topology.[29] If the radius is sufficiently small compared to the mesh size, regular Brownian diffusion is expected. Once the particle radius approaches the mesh size, the particles can experience the gel topology and have been reported to undergo anomalous, non-Brownian behavior where particles "hop" from areas of low crosslink density to regions of lower crosslink density in highly heterogeneous polyacrylamide networks.[26,30]

Fluorescence correlation spectroscopy super-resolution optical fluctuation imaging (fcsSOFI) can be used to investigate diffusion dynamics in gel environments to further understand how complex systems like the ECM affect these dynamics.[31–36] Developed by Kisley et al., fcsSOFI temporally correlates the signal from diffusing particles spatially at each pixel in wide field microscopy data to simultaneously map where particles are diffusing and quantify spatial distribution of heterogeneous diffusion constants. Compared to particle tracking methods, fcsSOFI super-resolves dynamic information with low signal data from relatively fast (>1–10 μm^2 s^{-1}) particle diffusion

within ECM-like environments such as agarose hydrogels and nanochannel substrates that are used in cell culture.[31,33,36] In increasingly dense networks, particle trapping and lower diffusion coefficients are observed.[32] For dextran ranging from 76 kDa to 2000 kDa in size in heterogeneous agarose gels with a pore size distribution of 300 ± 100 nm, smaller dextran molecules move more freely in small gel pores and can map detailed gel structure, while larger dextran molecules are confined and highlight only larger pores.[31,36] Overall, the fcsSOFI technique can characterize local nanoscale diffusion dynamics as opposed to the bulk dynamics in gel environments and is highly sensitive to the network topology.

In addition to controlling transport and diffusion, networks have also recently been found to stabilize protein organization in synthetic[37,38] and cell environments due to a balance of elastic deformation and enthalpic drive for phase separation[39,40] and to control the structure of collagen.[41] Phase separation of proteins results in spatial organization in networks. Elastic stresses limit the size scales of phase separated droplets and may control the thermodynamics of phase separation. Recently, Wilcox et al.[42] formed complex coacervates inside of polymer gels to investigate how elastic stresses affect systems similar to biocondensates found in the elastic environment of the cytoplasm. The study found that increases in gel modulus resulted in smaller complex coacervates and higher polyelectrolyte concentration in the complex coacervate phase. In another study, Lane and Weiss found that tissues with the smallest diameter collagen fibrils (<60 nm) have the highest concentration of the articular cartilage extracellular matrix which may translate to higher crosslinking densities.[9] Gobeaux et al. have also found that in dense collagen gels (40–300 mg mL^{-1}), collagen structure changes as a function of gel concentration. In 10 mg mL^{-1} gels, the diameter of collagen type I fibrils is reported to be 20–40 nm. The diameter increases to 40–120 nm as the concentration goes to 80 mg mL^{-1} and peaks at 1.5 μm in 90–150 mg mL^{-1} gels before decreasing again in concentrations higher than 200 mg mL^{-1}.[41] In this way, the gel environment has been shown to control phase separation and self-assemblies of proteins.

We study the structure and diffusion of collagen in polyacrylamide gels to investigate the role of the matrix elasticity on self-assembly and dynamics. Collagen fibrils are formed in gels of increasing modulus from 63–8900 Pa. Through total internal reflection fluorescence (TIRF) microscopy, highly inclined and laminated optical sheet (HILO) microscopy, and cryogenic transmission electron microscopy, we are able to determine how the gel network effects fibril formation and fibril bundle size. We use fcsSOFI to study the diffusion dynamics of collagen triple helices prior to fibril formation in the gels to investigate the mode of transport and mechanism of assembly. We observe that local elastic effects can lead to hierarchical changes in protein fibril formation that is relevant to many biological tissues.

Materials and methods

Sodium phosphate dibasic dodecahydrate, potassium dihydrogen phosphate, sodium chloride, and glacial acetic acid were

purchased from Sigma Aldrich. Sodium carbonate, sodium bicarbonate, and dimethyl sulfoxide (DMSO) were purchased from Fisher Chemical. AZ Dye 488 TFP ester (AZ488) was purchased from Vector Labs. All solutions were made using deionized water from a Milli-Q Direct 8 system with a resistivity of 18.2 MΩ cm and/or protocol with a resistivity of ≥10 MΩ cm. Solutions of 100 mM phosphate buffered saline (PBS) were prepared using 25 mM phosphate salts and the remaining 75 mM from sodium chloride to produce a buffer solution of pH 7.4. pH 2 solutions were prepared by diluting 12 M HCl from Fisher Chemical to 0.012 M HCl. All solutions were adjusted to ±0.02 of the desired pH using a pH meter and a few drops of dilute HCl and sodium hydroxide purchased from Fisher Chemical and Fisher Scientific.

Similar to the previous study by Wilcox et al.,[7] purified type II collagen from bovine nasal septum was purchased from Elastin Product Company. This materials is fully characterized by Wilcox et al.,[7] including the molecular weight (260 000 ± 50 000 g mol^{-1}) and fibrillar self assembly in different ionic environments using transmission electron microscopy (TEM). As noted previously,[7,43] the collagen was extracted from the native tissue using guanidine–HCl and treated with pepsinized acetic acid at pH 3.0 to then stabilize the collagen. To isolate collagen type II and purify the solution, fractional precipitations with NaCl, precipitations by dialysis against Na_2HPO_4, and column chromatography was used by the vendor.

Collagen solution preparation

In a process similar to the previous study by Wilcox et al.,[7] all soluble collagen solutions were prepared by dissolving type II collagen in 0.012 M HCl. The 1 g L^{-1} collagen solution was mixed for 3 hours on a stir plate at room temperature to allow the collagen to fully dissolve. The solution was then centrifuged for 30 minutes at 13 400 rpm (12 100 × g) in an Eppendorf 5452 "mini spin" centrifuge to separate any impurities in the system.[44] After centrifugation, the solution was stored at 4 °C for 48 hours until subsequent experiments. These filtered solutions were used for fluorescent conjugation, gel samples, and structural analysis of collagen with TEM and cryogenic electron microscopy (cryo EM).

When preparing collagen fibril solutions in pH 7.4 PBS solutions, the 1 g L^{-1} collagen solution in HCl was added to the intermediate pH buffer solution so that the final collagen concentration was 0.1 g L^{-1}. The collagen buffer solutions were left undisturbed for 48 hours at room temperature to form fibrils. The solutions were then centrifuged for 30 minutes at 13 400 rpm to separate the collagen fibrils from the collagen triple helices. 80% by volume of the remaining liquid was removed, and the remaining collagen fibrils were stored in a refrigerator at 4 °C overnight to 72 hours until subsequent microscopy imaging. The final concentration of collagen was 0.4 g L^{-1}, and the fibrils in the pallet were imaged with TEM.[7] This concentration is similar to the concentration of collagen in gels used in this study.

Polyacrylamide gel preparation

To prepare collagen inside of polyacrylamide gels, a modified process from Wilcox et al.[42] was used. The gel modulus was controlled by changing the ratio between the monomer, acrylamide, and the crosslinker, N,N′-(1,2-dihydroxyethylene)-bisacrylamide, which will subsequently be referred to as bisacrylamide, in a procedure similar to that of Sheth et al.[45] The full list of ratios for each formulation used can be found in Table 1.

Pre-gel solutions were made by initially mixing specified amounts of 40% by mass acrylamide and 0.5% by mass N,N′-(1,2-dihydroxyethylene)bisacrylamide in 0.012 M HCl solution. Specified concentrations and volumes of collagen solution were also added such that the final collagen concentration within the total pre-gel solutions were 0.75 mg mL^{-1} (Fig. 1). A photoinitiator, 2-hydroxy-4′-(2-hydroxyethoxy)-2-methylpropiophenone, was then added at 2.4–8 mg per mL of total pre-gel solution. The mixture was stirred at room temperature, and the resulting solution was filtered using a 0.45 µm PES syringe filter from MDI. To gel, the pre-gel solution was irradiated for 30 minutes using a 365 nm wavelength 6-Watt UV lamp. After the gel was formed, the gel was soaked in 100 mM PBS solution for two days at room temperature (Fig. 1). Gels were stored at 4 °C in a refrigerator for 3 days prior to electron microscopy imaging. Then, working in an ice bath to prevent further fibrillogenesis in vitro and to ensure repeatability, the surface of the gel was dried using a KimWipe. The gel was rinsed in a 9:1 100 mM PBS to 0.012 M HCl solution and placed in 1 mL of a 9:1 100 mM PBS to 0.012 M HCl solution. For cryogenic transmission electron microscopy (cryo-TEM), the gels were mechanically broken up using a syringe and needle to produce a gel slurry that could be easily placed on the cryo-TEM grid in lieu of other chemical or additional freezing methods.

Tagging collagen

In order to investigate the effect of environmental elasticity on the assembly of collagen fibrils, collagen was tagged with fluorescent dyes using a procedure similar to Siadat et al. that tagged collagen type I.[46] Collagen type II was dissolved at 1 g L^{-1} in 0.012 M HCl and mixed for 3 hours. The solution

Table 1 Acrylamide and bisacrylamide ratios in 0.012 M HCl and resulting gel properties

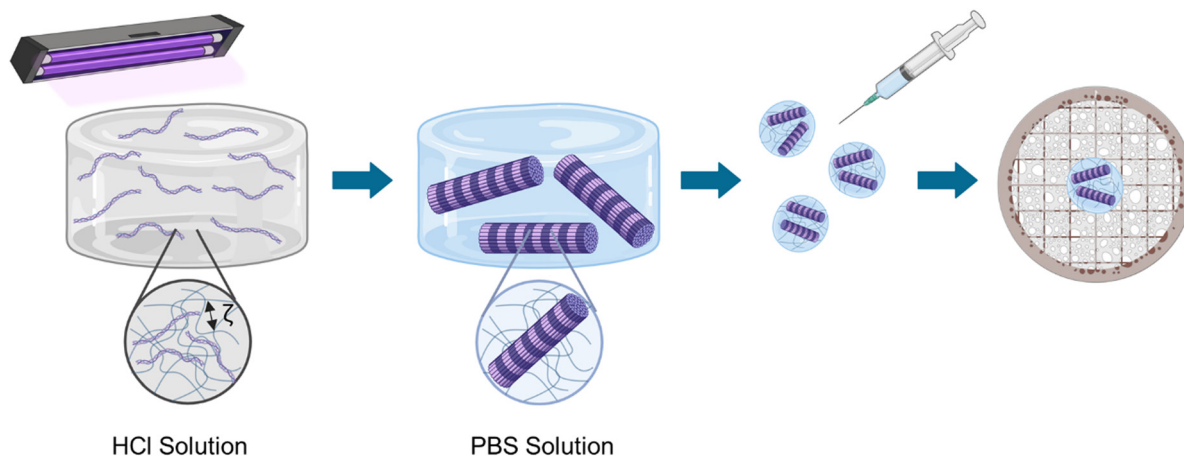| Formulation name	Acrylamide (wt%)	Bisacrylamide (wt%)	Acrylamide stock (mL)	Bisacrylamide stock (mL)	Collagen (mg mL^{-1})	Gel G' (Pa)	Gel mesh size (nm)
A5B.08	5	0.08	0.625	0.200	0.90	63	40
A5B.1	5	0.1	0.625	0.250	0.91	460	21
A8B.1	8	0.1	1.000	0.250	1.00	570	19
A8B.25	8	0.25	1.000	1.000	1.25	1040	16
A15B.75	15	0.75	2.000	2.000	1.00	8900	7.8

Fig. 1   A visual representation of the process used to make collagen fibrils within polyacrylamide gels and making samples for cryo-EM. First, an aqueous 0.012 M HCl solution of acrylamide, bisacrylamide, collagen, and a photoinitiator is exposed to UV light to induce gelation. The result is a network of a particular mesh size, ξ, depending on the concentrations. Mesh size is denoted by the black arrows. The gel is subsequently placed in a 100 mM PBS solution to form fibrils, then broken up into a slurry using a syringe and needle with 1 mL of PBS solution. Finally, the gel slurry is deposited onto a cryo-EM grid.

was then centrifuged at 13 400 rpm (12 100 × g) for 30 minutes to separate any impurities in the system.[44] The supernatant was removed and stored at 4 °C in a refrigerator for 48 hours. For the tagging reaction, the 1 g L^{-1} collagen solution was mixed in equal volume with a pH 9.6, 0.2 M sodium carbonate–bicarbonate buffer containing 1 M NaCl so that the collagen concentration was 0.5 g L^{-1}. A 0.5 mg mL^{-1} solution of AZ Dye 488 TFP ester in DMSO was then added to achieve a weight ratio of 0.2 mg of dye for every 1 mg of collagen in the starting solution. This proportion allows for 1.1 mole of dye for every 1 mole of lysine in the collagen. Should all lysine moieties be tagged, then 4% of the collagen triple helix will subsequently be tagged. The reaction was carried out at room temperature and stirred for 3 hours. Once the reaction time was complete, an equal volume of 1 M acetic acid containing 1.3 M NaCl to the reaction volume was added to precipitate the collagen so that the total collagen concentration was 0.42 g L^{-1}. The solution was then centrifuged for 1 hour at 7830 rpm (30 130 × g) in an Eppendorf 5430 centrifuge, after which the supernatant was removed. 0.012 M HCl was added to the remaining precipitate to redissolve the collagen overnight in at 4 °C within a refrigerator. The solution was then filtered to remove excess dye through 10 kDa molecular weight cutoff Spin-X® UF concentrator spin columns from Corning at 7830 rpm for 30 minutes. The spin purification process was repeated six times, and the original solvent was replaced by a 0.012 M HCl solution after each round of purification. The final concentration of the tagged collagen was 1 g L^{-1} and was stored in a freezer until use.

Electron microscopy

Electron microscopy techniques were used to visualize and determine the diameter of collagen fibrils at nanometer scales. To gain better resolution and contrast, transmission electron microscopy (TEM) was used. However, as TEM can only image collagen fibrils in a dried state, cryo-TEM was used to observe

hydrated collagen fibril diameter and structure in solution and within gel environments. We anticipate only minimal assembly due to vacuum since the solutions were not dried onto the sample grid.

Fibril diameters were approximated using the intensity profiles of the images. To measure diameters, intensity profiles across multiple fibrils were obtained using ImageJ. The diameter was recorded as the width at half-height of the intensity profile (Fig. S7, ESI†).

Transmission electron microscopy

For TEM imaging, 10 μL of a 0.4 g L^{-1} collagen fibril solution were added to a 400 mesh Cu grid coated with Formvar for 45–135 seconds. This solution was made by centrifuging down a 0.1 g L^{-1} pH 7.4 collagen solution, and 80% of the supernatant removed. The grid was then rinsed with a buffer solution and then a 2% uranyl acetate stain. After being exposed to the stain for 45–135 seconds, the excess stain was blotted off. Samples were imaged under vacuum using a Tecnai T12 electron microscope at 80 kV and a Tecnai F20 electron microscope at 200 kV.

Cryogenic transmission electron microscopy

Cryo-TEM is used to image many different soft matter systems.[47] For cryo-TEM imaging, 4 μL of 0.4 g L^{-1} collagen fibril solution or gel slurry were added to a 300 mesh Cu lacey carbon with approximately 63 μm grid hole size (Fig. 1). The total collagen number in all gels was kept constant. The grids were then blotted with −5 to 15 units of force. After 10 s, the girds were plunged and flash frozen in liquid ethane in a Vitrobot that was maintained at 4 °C and 100% humidity. Samples were then imaged under vacuum using the Tecnai F20 electron microscope at 200 kV in low dose mode.

Rheology

Rheology measurements were performed using a procedure similar to Wilcox et al.[42] to determine the gel modulus and

strain behavior. Oscillatory frequency sweep measurements were performed on a ThermoFisher Scientific HAAKE MARS III rheometer at a small strain amplitude (γ = 5%) in an angular frequency (ω) range from 1 to 10 rad s^{-1} to determine the storage modulus, G', and loss modulus, G''. Measurements were taken using a 20 mm parallel plate geometry at room temperature. Gap height varied between 1.2 to 2.25 mm as gel heights between samples varied by the extent of swelling. G' was determined by the average of 3–4 trials of the oscillatory frequency sweeps at low strain. Oscillatory amplitude sweep measurements were used to probe gel strain behaviors from 5% strain until gel breakage was observed.

Optical microscopy

Plain coverslips (no. 1.5 22 mm × 30 mm) were purchased from Corning. The no. 1.5 coverslips were cleaned by submerging the glass in ultrapure type I water purified on an Elga Chrous 2+ system, followed by boiling in basic piranha solution (TL1, 6 : 1 : 1 (v/v) ratio of H_2O : H_2O_2 : NH_4OH) at 75 °C for 2 minutes. The coverslips were then rinsed with ultrapure water and dried with ultrapure N_2 (Airgas) before being treated in an O_2 (Airgas) plasma cleaner (Harrick Plasma) at 11 W for 2 min.

After the gel samples were soaked in 0.012 M HCl solution for 1 hour to reach swelling equilibrium, samples were imaged using a custom-built TIRF microscope previously described.[48] First, the gel was imaged after soaking in the HCl to determine the collagen monomer diffusion in the gel followed by transferring it to the pH 7.4 PBS solution to initiate fibril formation. The solution volume was at least 20 times the gel volume. The gel was taken out of the PBS solution and imaged at specific time points as mentioned in the figure panels. The setup includes an Olympus IX83 microscope body and a 100×/1.49 NA oil immersion TIRF objective lens (Olympus) for sample excitation and imaging. A 488 nm laser (Toptica Photonics) was used to excite all samples, with a laser power density of $\sim$62 W cm^{-2}. Imaging modes were switched between TIRF, to image just below the surface of the gels, and HILO, to image deeper within the sample.[49,50] The HILO imaging mode was set by positioning the TIR lens so that the incident angle of the laser is slightly lower than the critical angle used in the TIRF mode. By approaching the back pupil of the objective below the critical angle, total reflection is not achieved. Instead, the beam exits the objective at an angle, effectively forming a light-sheet. The image collection settings were managed using Micro-Manager 2.0, capturing images on either the full chip (1412 pixel × 1412 pixel) for single frames or a subsection (100 pixel × 100 pixel) for multi-frame datasets of a Photometrics Prime 95B 22 mm sCMOS camera. For both regions of interest, the exposure time was set to 5 ms (200 fps).

All data were analyzed using our fcsSOFI code, which is publicly available on GitHub.[34] In general, this code generates a SOFI image and a FCS diffusion map, then combines the two to provide both structural and diffusion information for a given sample.[32] After generating diffusion data for a sample for each pixel in the 100 pixel × 100 pixel array, we generate a cumulative distribution of all diffusion coefficients at each pixel. The

mean diffusion coefficient (D) is determined by fitting the cumulative distribution points to a normal cumulative distribution error function, CDF:

$$\text{CDF} = \frac{1}{2}\left(1 + \text{erf}\left(\frac{x - \mu}{\sigma\sqrt{2}}\right)\right) \tag{1}$$

where μ represents the mean D of the data set and σ is the slope of the curve.

Results and discussion

We have determined the structure and diffusive dynamics of collagen type II in polyacrylamide gels as a function of increasing modulus from 63–8700 Pa. Collagen fibrils and fibril bundles are formed in these gels in a process summarized by Fig. 1. Briefly, collagen type II is dissolved in acidic conditions in the presence of acrylamide and bisacrylamide monomers. After curing the network, the solvent is exchanged to a neutral pH to promote fibril formation. To determine the resulting structure, collagen is imaged using cryo-TEM. TIRF and HILO microscopy are used to further qualitatively verify the observed structures. To determine dynamics, fcsSOFI is used to calculate soluble fluorescently tagged collagen diffusion coefficients within solution, a soft gel ($<$1000 Pa), and a stiff gel ($>$1000 Pa). Overall, we observe that the gel topology can limit the collagen fibril size and slow the dynamics of collagen fibril assembly.

Representative cryo-TEM images of individual fibrils and fibril bundles are shown in Fig. 2. Faint D-banding and twists are observed in both solutions and gels (Fig. S10–S12, ESI†), so the observed fibrillar assemblies are assumed to be collagen fibrils. In TEM, single fibrils are identified by the D-banding of the fibrils, which are typically $\sim$67 nm and appear as striations that run perpendicular along the length of the fibril.[51,52] Fibril bundles are multiple fibrils twisting around each other or are greater than 100 nm in diameter (Fig. S11, ESI†). We do not observe molecular aggregation in the previously published TEM samples, and assume that all structures are collagen fibrils even if the contrast is not high enough to observe striations. In addition, the fibrillar features are similar to previously imaged collagen fibrils in solution with EM.[53] Histograms are also reported in Fig. 2. For the histograms, the number of fibrils and fibril bundles measured was 69 for the collagen assembled in solution and 90, 75, 33, 24, and 32 for collagen assembled in gels in order of increasing modulus. The fibril diameter was determined using the full width at half maximum of a representative line section of the fibril in ImageJ as shown in Fig. S7a (ESI†). These images were not altered in any way aside from the addition of scale bars in ImageJ. We observe that the fibrils and fibril bundles in solution are smooth in appearance while the structures in gels have looser organization and are "wispier" in appearance.

In polyacrylamide gels, the distribution of collagen fibril diameters (including fibril bundles and single fibrils) narrows as a function of increasing modulus (Fig. 2). Fibril bundles in solution have a skewed distribution with the most bimodal distribution and a dominating large shoulder. The gel network
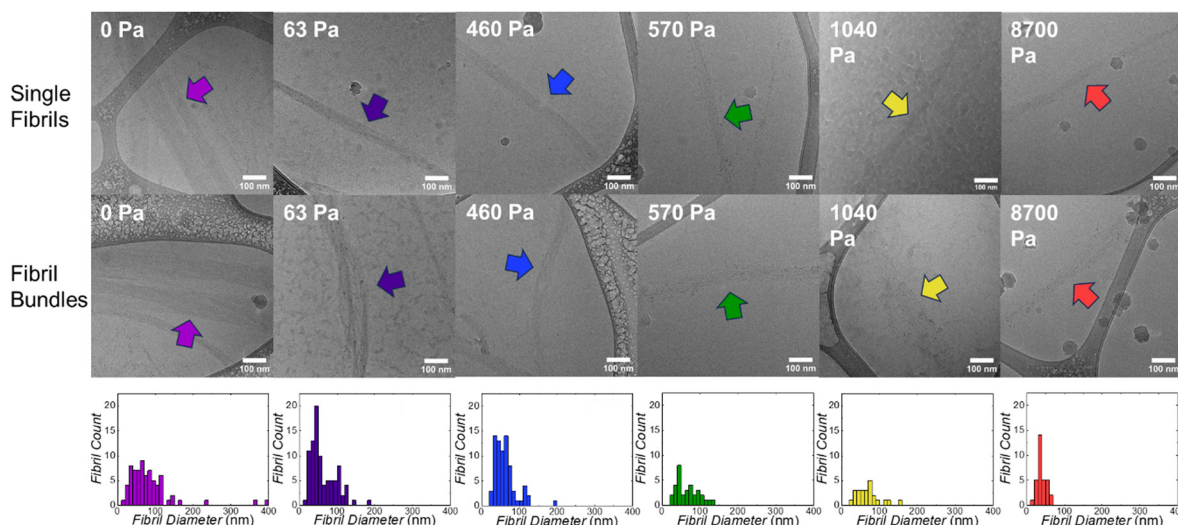
Fig. 2 Representative cryo-TEM images of single collagen fibrils and collagen fibril bundles in solution and polyacrylamide gels. 0 Pa designates structure in solution. Accompanying histograms are of the combined single collagen fibrils and fibril bundles in solution and polyacrylamide gels. The arrows indicate the location of fibrils or fibril bundles within the image.

appears to restrict larger fibril bundle formation with increasing modulus. A bimodal distribution can also be seen in the softest gel with a modulus of 63 Pa. The total number of fibril bundles decreases with increasing modulus until only a single distribution is observed in the highest modulus gel (8700 Pa). In 570 Pa networks, only 5 of 33 structures are observed that have a diameter greater than 100 nm and in 1040 Pa networks, only 3 of 24. In the 8700 Pa networks, we observe mostly individual fibrils. Collagen forms fibrils in all gels, but in soft gels ($G' <$ 1000 Pa) fibrils tend to have bimodal distributions while mostly single fibrils are observed in stiff gels ($G' >$ 1000 Pa).

In order to compare with previous studies,[7] the images were analyzed to separate out single fibrils. The results are summarized in Fig. S7b (ESI†), with additional TEM images from Wilcox *et al.*[7] In solution, the single fibril diameter is approximately 47 nm while in polyacrylamide gels, the fibril diameter is ~30 nm across three orders of magnitude of gel moduli (Fig. 3). Fig. S7 (ESI†) shows the histograms for all single fibril measurements where the number of single fibrils measured for solution conditions is 27 from TEM images and 31 from cryo-EM images. For each gel, 85, 31, 49, 33, and 34 fibrils were analyzed from cryo-EM images in order of increasing modulus. The histograms are consistent with normal distributions and do not change as a function of gel modulus. We do find that the distribution of the single fibrils in solution is significantly wider than the distributions of single fibrils in any gel modulus. The standard deviation decreases from 18 nm in solution to 8.9 ± 2.5 nm across the gels of varying modulus. This effect is likely due to confinement properties of the network, or a change in the solution interactions. It has been previously suggested that collagen fibril thicken over time, and the presence of the network as well as the complex dynamics within the network would limit this process.[54]

Optical microscopy qualitatively agrees with cryo-TEM results. As shown in Fig. 4, there are fewer fibril bundles in representative stiffer gels (G' = 3400 Pa) than in softer gels (G' =
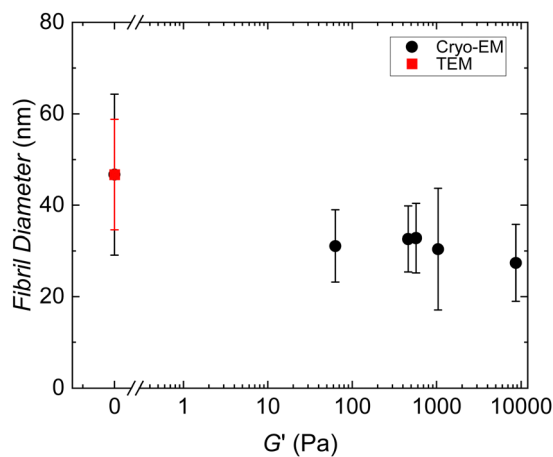

Fig. 3 Analysis of single collagen fibril diameter in solution and gels as a function of gel modulus. The 0 Pa modulus is designated as the solution condition.

500 Pa) (Table S1, ESI†). In the soft gels, fibrils formed within 30 minutes and could be seen scattered throughout the gel and increased in size during the 48-hour study. In the stiff gel, shorter fibrils also formed within 30 minutes, but were scarce throughout and did not noticeably increase in size even after 48 hours soaking in the PBS buffer. Moreover, we see less and slower fibril formation in the collagen solution samples compared to the softer gel matrix (Table S1, ESI†).

While fibrils could be observed in either gel as soon as 15 min after soaking in the PBS buffer, fibrils were not observed in the PBS solution until after 3 hours. This discrepancy between the solution and gel environments is due to the non-equilibrium state of fibril formation. There are also other factors that can lead to variability in the results. First, the concentration of collagen is variable between the three environments. After the gels are produced and placed in the soaking solutions of similar volumes,
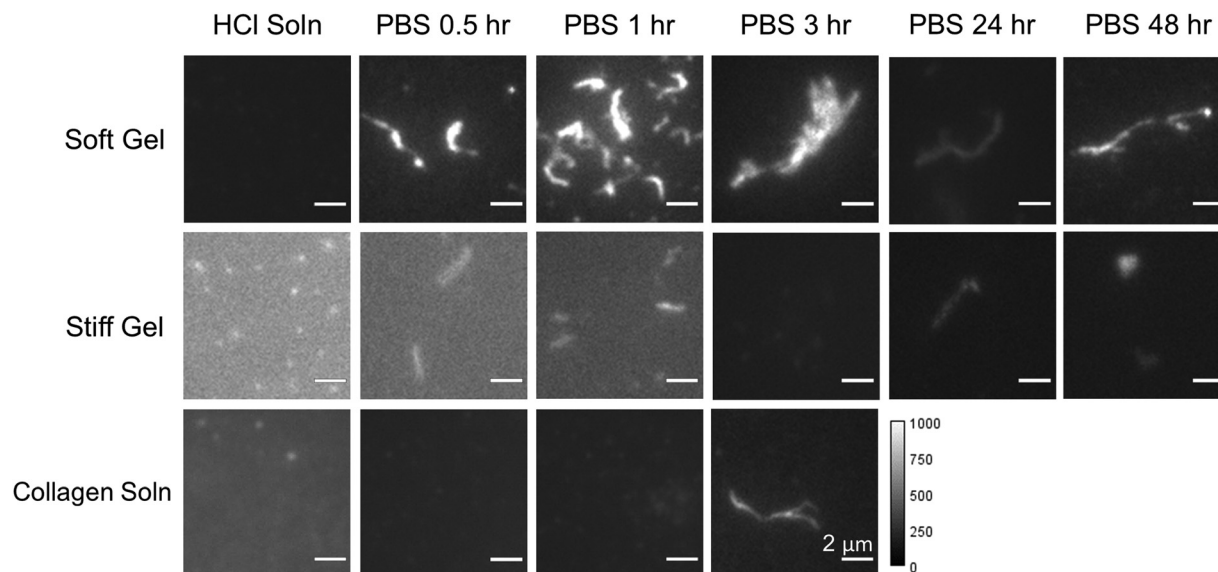
Fig. 4 Optical microscopy images of AZ488 tagged collagen in the soft (G' = 500 Pa), the stiff (G' = 3400 Pa) gels and in solution at 0.11 g L^{-1} using HILO and TIRF, respectively. Scale bars are 2 μm. Colorbar represents camera intensity, which is kept constant for each image.

they swell, thereby decreasing the collagen concentration. For the soft gels, the swelling approximately doubles the gel volume (specifically by a factor of 1.5–2.2), which decreases the collagen concentration by half. In contrast, the swelling of stiff gels is negligible with little change to the overall starting gel concentration. However, collagen can also diffuse out of the gel during soaking, varying the overall concentration between gels of the same modulus. Second, comparing only the gels, the difference in the modulus could impact collagen transport as it starts to form larger bundles. A stiff gel will be considerably more crosslinked and have smaller mesh-sizes, effectively trapping the collagen and collagen fibrils. Finally, gel interactions could potentially drive or hinder collagen formation and would depend on the local polyacrylamide concentration.

In addition to any non-equilibrium concentration fluctuations that happen upon solvent change, collagen fibrillogenesis has been previously reported to depend on the local ionic strength and temperature. Typically, the kinetics are characterized by the time necessary for the turbidity of the solution to change. For collagen type II in 126 mM ionic strength, this time has been reported to be on the order of 5 minutes.[55] The period of saturation can last up to 30 minutes. While turbidity is a measure of the entire sample, we measure fibrillogenesis locally, within 100 μm, where any heterogeneity can drastically affect the growth of fibrils locally. AFM studies on the longitudinal and lateral growth mechanisms of collagen also show that while generally fibrils can be seen within 6 minutes, the surface coverage is below 10% until ∼30 minutes even for the highest concentrations studied.[54]

Comparing the diffusion coefficients for soluble collagen type II in solution, the soft gel (G' = 500 Pa), and the stiff gel (G' = 3400 Pa), there is a clear trend that links the diffusion speed to the confinement of the environment (Fig. 5). In these experiments, the collagen is not yet in fibrillar form, since as

fibrils start to assemble, diffusion slows and becomes difficult to resolve. For collagen in the HCl solution prior to fibrillogenesis *in vitro*, the diffusion coefficient is 4 ± 1 μm^2 s^{-1} which correlates to a hydrodynamic radius of ∼55 nm based on the Stokes–Einstein equation.[56] According to differential dynamic microscopy (DDM) and dynamic light scattering (DLS) (Fig. S5, ESI†), the diffusion coefficient of tagged triple helices in HCl is approximately 7 μm^2 s^{-1} and within a similar order of magnitude. After the collagen is introduced to PBS buffer, the diffusion slows to 2.3 ± 0.8 μm^2 s^{-1}. At 15 minutes in PBS, the Brownian motion steadily decreases until no fluctuations can be observed after 3 hours using our technique (Fig. 5A). Since the viscosity of the HCl and PBS solutions are similar, the slower diffusion coefficient indicates fibril formation, with an increase in hydrodynamic radius to ∼100 nm. The corresponding fcsSOFI images in solution (Fig. 5B and C) show that collagen and fibrils are able to access the entire area of the sample. Fig. 5B and C show heatmaps of the location and rate of diffusion. Higher saturation areas indicate more fluctuations and local accessibility of the gel to collagen where motion is present even if the average concentration of collagen in the entire field of view of both systems is similar as shown in the supplementary movies (ESI†). There is quantifiable diffusion at all pixels (bright areas in Fig. 5B and C) in acidic conditions and a decrease in the diffusion coefficient after 30 min in PBS, observed as a change in the color of the image.

In the gels (Fig. 5D–H), the diffusion of the collagen slows compared to in solution and slows further after triggering fibril formation in neutral pH. The diffusion coefficients in the HCl soaked gels are 3 ± 1 μm^2 s^{-1} and 3 ± 2 μm^2 s^{-1} for the soft and stiff gels, respectively, and can be seen in Fig. 5D–H. Notably, the average D is similar despite the gel polyacrylamide concentration and modulus. Further inspection of all D values in the stiff gel shows a wider range of and less Gaussian distribution, with a higher population of slower diffusion (Fig. 5G) compared
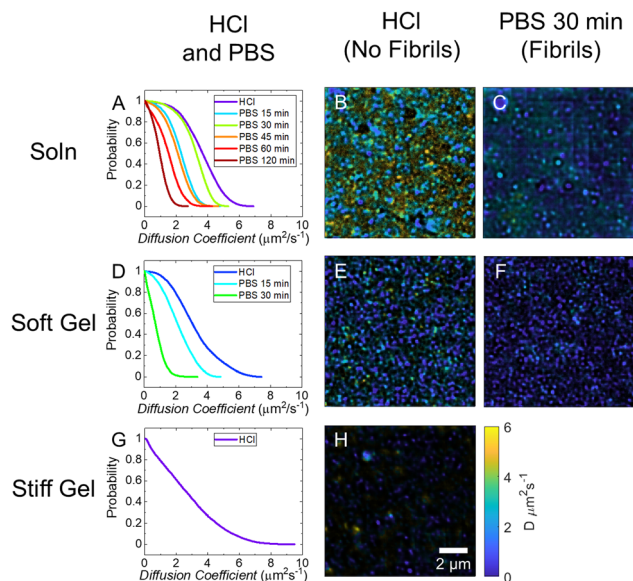
Fig. 5 Optical analysis of collagen diffusion in solution and gels. (A), (D) and (G) Cumulative distributions of the measured diffusion coefficients of the AZ488 tagged collagen in 0.012 M HCl at time points in PBS for solution and gels. (B), (E) and (H) Representative fcsSOFI images of AZ 488 tagged collagen in HCl environments in solution and gels. (C) and (F) Representative fcsSOFI images of AZ488 tagged collagen in PBS environments in solution and gels at 30 minutes in PBS when collagen fibrils have formed.

to the soft gel. After soaking in PBS solutions, the motion slows as fibrils form (Fig. 5D). This slowing has also been seen in *Escherichia coli* in porous media studies by Bhattacharjee and Datta.[57] In both gels, with increasing time in PBS, we found fewer diffusing collagen. While we were able to observe motion in the soft gel up to 30 min soaking in PBS, we were only able to collect data for the stiff gel prior to any fibril formation. Spatially, the fcsSOFI images show that for the soft gel, collagen prior to fibril formation has similar accessibility within the polyacrylamide as in solution, with diffusion observed throughout the gel (Fig. 5E). As fibrils form upon PBS soaking, accessibility is decreased within the gel as denoted by a combination of an increase in the black areas from 21 664 pixels in Fig. 5E to 22 679 pixels in Fig. 5F. In contrast, the collagen is limited to distinct pockets in the stiff gel even prior to fibrilization, as observed by the mostly black areas in Fig. 5H.

Interestingly, the mode of diffusion for the collagen fibrils qualitatively appears to change in polyacrylamide gels (Videos S1–S5, ESI†). When allowed to freely diffuse within the solution environment, the diffusion appears to be Brownian in nature both in HCl and PBS solutions (Videos S1 and S2, ESI†). However, within the gel environments, the diffusion appears to be more of a "hopping" motion (Videos S3–S5, ESI†), which has previously been described as a type of anomalous diffusion.[58] The "hopping" motion is similarly described in previous work as the movement of particles from one pore to another in a highly crosslinked network where the particle size is similar to that of the mesh.[30,59,60] The change in the mode of diffusion is captured as a reduction in the diffusion coefficient, but the mechanistic behavior is difficult to quantify solely with D using our fcsSOFI code.

We observe that collagen forms fibrils in polyacrylamide networks across three orders of magnitude. While the radius of individual fibrils remains constant at ~ 30 nm, the distribution of all higher order structures appears to have a strong dependence on the network modulus. The average diffusion coefficient of soluble collagen triple helices is also similar in both soft and stiff gels. We interpret these results in terms of the network topology. The heterogeneity, not the average mesh size, of the polyacrylamide network must be considered to understand the observed structure and dynamics of collagen. Using storage modulus, G', the mesh size, ξ, of the gel can be estimated by the equation:

$$G' = \frac{k_B T}{\xi^3} \qquad (2)$$

where k_B is the Boltzmann constant and T is the temperature (Table 1). A visual representation of the mesh size can be seen in Fig. 6A. The range of the average mesh size of the network varies from 40 nm for the 63 Pa gel to 7.8 nm for the 8700 Pa gel. However, the diameter of collagen fibrils is limited to ~ 30 nm, and fibril bundles are on average ~ 100 nm in diameter, which is larger than the mesh size of most of the gels. Because of the chemistry of the polymerization of polyacrylamide gels used in this study, the gel topologies are heterogeneous with areas of high and low crosslink densities. In previous studies, these less densely crosslinked regions have been described as "pores" with diameter $d_p \sim 100$ nm in size (Fig. 6A). We expect that the fibrils form in areas containing larger pores along a path of least resistance (Fig. 6B). This is evident from the resulting structure as well as the apparent diffusion in the gels studied. The preference for collagen fibrils to form in larger than average pores would explain how single fibril diameters of ~ 30 nm form in $G' = 8700$ Pa gels that have an average mesh size of 7.8 nm and fibril bundles with diameters in 100 s of nanometers to form in the softest gels that have average mesh sizes of ~ 20–40 nm. In addition, the fibril diameter has a narrower distribution in the stiffest gel due to the gel environment. In these networks, we observe generally less collagen motion in fewer parts of the network. From optical microscopy, we observe fewer and thinner fibril bundles in stiff gels than in soft gels with collagen diffusing in either gel at similar rates. Overall, single collagen fibril diameter is limited by the gel network regardless of the gel modulus. Collagen diffusion is also independent of the network, so most likely, structure forms in areas of low crosslinking density.

Conclusions

We have studied collagen type II fibril structure and dynamics in solution and in 63–8700 Pa polyacrylamide gels. Fibril diameters were analyzed using cryo-TEM and optical fluorescence microscopy. From these methods, we have determined that the single fibril diameter is limited by the gel network to ~ 30 nm and is independent of gel modulus while fibril bundles are constricted by the stiff gel networks. In gels, the
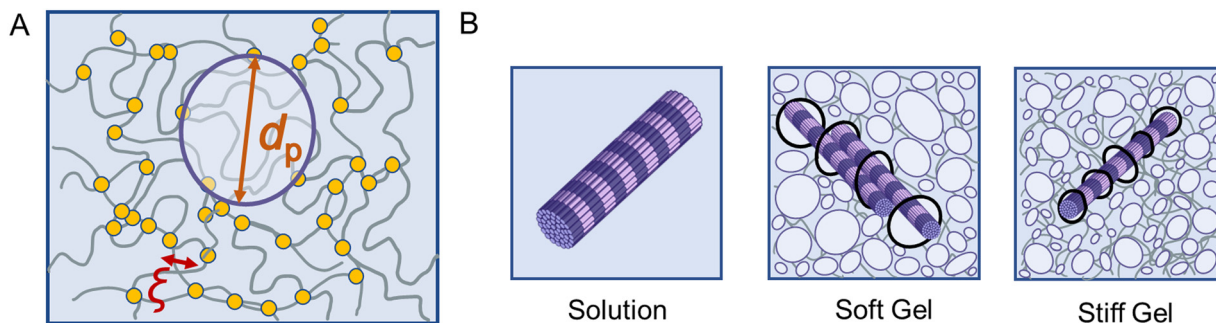
Fig. 6 Collagen fibrils in comparison to mesh size. (A) Mesh size, ξ, as denoted by the red arrows, is heterogenous throughout the gel that has regions of high crosslink density and low crosslink density. Pore size is a larger length scale associated with areas of lower crosslink density, of average size d_{p}. (B) Schematic of collagen fibrils grown in solution, the softest gel, and the stiffest gel. The variance in the pore sizes of each gel leads the fibrils to grow within the larger pores as they provide a path of least resistance (highlighted with black outlines). In soft gels, bundles are also observed due to higher pore sizes.

diffusion of collagen is slower when compared to that in solution, but the average rate of soluble collagen diffusion is independent of the gel modulus. Due to the minimal dependence of both structure and dynamics on the matrix strength and concentration, the fibrils likely form in a path of least resistance within the heterogenous topology of the gel network. By understanding how elastic networks influence the hierarchical changes in protein fibril formation, we set foundations for improved extracellular matrix model materials and synthetic tissues.

Author contributions

K. W., S. C., S. K., L. K., and S. M. designed the research. K. W. and S. S. prepared the samples. K. W. performed the TEM and cryo-EM experiments, analysis, and write-up. S. K. and S. C. preformed the light microscopy experiments and analysis. S. K. wrote up the light microscopy experiment results and analysis. A. L. preformed rheology experiments and analysis. All authors reviewed the final manuscript.

Data availability

All raw rheology curves and description and examples of image analysis are found in the ESI.† All raw cryo-TEM images and microscopy movies can be downloaded can be found on Dryad: **https://doi.org/10.5061/dryad.cc2fqz6g6**. Code for microscopy analysis that was used to track diffusion and location of collagen in gels is available on GitHub: **https://github.com/KisleyLabAtCWRU/fcsSOFI**.

Conflicts of interest

There are no conflicts to declare.

Acknowledgements

Notes and references

1 S. N. Deshmukh, A. M. Dive, R. Moharil and P. Munde, Enigmatic insight into collagen, *J. Oral Maxillofac. Pathol.*, 2016, **20**(2), 276. Available from: **https://pmc.ncbi.nlm.nih.gov/articles/PMC4989561/**.

2 V. Ottani, D. Martini, M. Franchi, A. Ruggeri and M. Raspanti, Hierarchical structures in fibrillar collagens, *Micron*, 2002, **33**(7–8), 587–596.

3 M. D. Shoulders and R. T. Raines, Collagen structure and stability, *Annu. Rev. Biochem.*, 2009, **78**, 929–958.

4 S. Morozova, P. W. Schmidt, F. S. Bates and T. P. Lodge, Effect of poly(ethylene glycol) grafting density on methylcellulose fibril formation, *Macromolecules*, 2018, **51**, 9413–9421.

5 G. M. Grason and R. F. Bruinsma, Chirality and equilibrium biopolymer bundles, *Phys. Rev. Lett.*, 2007, **99**(9), 1–4.

6 G. M. Grason, Braided bundles and compact coils: The structure and thermodynamics of hexagonally packed chiral filament assemblies, *Phys. Rev. E: Stat., Nonlinear, Soft Matter Phys.*, 2009, **79**(4), 1–15.

7 K. G. Wilcox, G. M. Kemerer and S. Morozova, Ionic environment effects on collagen type II persistence length and assembly, *J. Chem. Phys.*, 2023, **158**(4), 044903. Available from: **https://aip.scitation.org/doi/abs/10.1063/5.0131792**.

8 A. J. Sophia Fox, A. Bedi and S. A. Rodeo, The basic science of articular cartilage: Structure, composition, and function, *Sports Health*, 2009, **1**(6), 461–468.

9 J. M. Lane and C. Weiss, Review of articular cartilage collagen research, *Arthritis Rheum.*, 1975, **18**(6), 553–562.

10 T. C. Laurent, Biochemistry of hyaluronan, *Acta Oto-Laryngol., Suppl.*, 1987, **442**(3), 7–24.

11 D. Eyre, Collagen of articular cartilage, *Arthritis Res. Ther.*, 2002, **4**(1), 30–35.

12 M. Ulrich-Vinther, M. Maloney, E. Schwarz, R. Rosier and R. J. O'Keefe, Articular cartilage biology, *J. Am. Acad. Orthop. Surg.*, 2003, **11**(6), 421.

13 K. G. Wilcox, S. K. Kozawa and S. Morozova, Fundamentals and mechanics of polyelectrolyte gels: Thermodynamics, swelling, scattering, and elasticity, *Chem. Phys. Rev.*, 2021, **2**(4), 041309. Available from: https://aip.scitation.org/doi/abs/10.1063/5.0048152.

14 S. Morozova and M. Muthukumar, Elasticity at swelling equilibrium of ultrasoft polyelectrolyte gels: comparisons of theory and experiments, *Macromolecules*, 2017, **50**(6), 2456–2466.

15 M.-M. Giraud-Guille and L. Besseau, Banded patterns in liquid crystalline phases of type i collagen: Relationship with crimp morphology in connective tissue architecture, *Connect. Tissue Res.*, 1998, **37**(3–4), 183–193. Available from: https://www.tandfonline.com/doi/full/10.3109/03008209809002438.

16 C. Salameh, F. Salviat, E. Bessot, M. Lama, J.-M. Chassot and E. Moulongui, *et al.*, Origin of transparency in scattering biomimetic collagen materials, *Proc. Natl. Acad. Sci. U. S. A.*, 2020, **117**(22), 11947–11953. Available from: https://pnas.org/doi/full/10.1073/pnas.2001178117.

17 Y. J. Yang, D. J. Mai, S. Li, M. A. Morris and B. D. Olsen, Tuning selective transport of biomolecules through site-mutated nucleoporin-like protein (nlp) hydrogels, *Biomacro-molecules*, 2021, **22**(2), 289–298.

18 F. Yuan, A. Krol and S. Tong, Available space and extra-cellular transport of macromolecules: Effects of pore size and connectedness, *Ann. Biomed. Eng.*, 2001, **29**(12), 1150–1158. Available from: https://link.springer.com/article/10.1114/1.1424915.

19 J. Záměčník, L. Vargová, A. Homola, R. Kodet and E. Syková, Extracellular matrix glycoproteins and diffusion barriers in human astrocytic tumours, *Neuropathol. Appl. Neurobiol.*, 2004, **30**(4), 338–350. Available from: https://onlinelibrary.wiley.com/doi/full/10.1046/j.0305-1846.2003.00541.x.

20 O. Lieleg, R. M. Baumgärtel and A. R. Bausch, Selective filtering of particles by the extracellular matrix: An electrostatic band-pass, *Biophys. J.*, 2009, **97**(6), 1569–1577. Available from: https://www.cell.com/article/S0006349509012284/fulltext.

21 S. Pajević, R. Bansil and Č. Koňák, Diffusion of linear polymer chains in methyl methacrylate gels, *Macromolecules*, 1993, **26**(2), 305–312. Available from: https://pubs.acs.org/doi/abs/10.1021/ma00054a009.

22 S. Seiffert, Origin of Nanostructural Inhomogeneity in Polymer-Network Gels, *Polym. Chem.*, 2017, **8**(31), 4472–4487, DOI: 10.1039/C7PY01035D.

23 S. Morozova, E. Hitimana, S. Dhakal, K. G. Wilcox and D. Estrin, Scattering methods for determining structure and dynamics of polymer gels, *J. Appl. Phys.*, 2021, **129**(7), 71101, DOI: 10.1063/5.0033414.

24 F. Ikkai and M. Shibayama, Inhomogeneity control in poly-mer gels, *J. Polym. Sci., Part B: Polym. Phys.*, 2005, **43**(6), 617–628. Available from: https://onlinelibrary.wiley.com/doi/full/10.1002/polb.20358.

25 M. Y. Kizilay and O. Okay, Effect of initial monomer concen-tration on spatial inhomogeneity in poly(acrylamide) gels, *Macromolecules*, 2003, **36**(18), 6856–6862. Available from: https://pubs.acs.org/doi/full/10.1021/ma021366u.

26 C. H. Lee, A. J. Crosby, T. Emrick and R. C. Hayward, Characterization of heterogeneous polyacrylamide hydro-gels by tracking of single quantum dots, *Macromolecules*, 2014, **47**(2), 741–749. Available from: https://pubs.acs.org/doi/abs/10.1021/ma402373s.

27 S. B. Chen, Dissipative particle dynamics simulation of nanoparticle diffusion in a crosslinked polymer network, *J. Phys. Chem. B*, 2022, **126**(37), 7184–7191, Available from: https://pubs.acs.org/doi/full/10.1021/acs.jpcb.2c05217.

28 L. H. Cai, S. Panyukov and M. Rubinstein, Hopping diffu-sion of nanoparticles in polymer matrices, *Macromolecules*, 2015, **48**(3), 847–862. Available from: https://pubs.acs.org/doi/full/10.1021/ma501608x.

29 K. Chen and M. Muthukumar, Entropic barrier of topologi-cally immobilized DNA in hydrogels, *Proc. Natl. Acad. Sci. U. S. A.*, 2021, **118**(28), e2106380118. Available from: https://www.pnas.org/doi/abs/10.1073/pnas.2106380118.

30 H. Wu and D. K. Schwartz, Nanoparticle tracking to probe transport in porous media, *Acc. Chem. Res.*, 2020, **53**(10), 2130–2139. Available from: https://pubs.acs.org/doi/abs/10.1021/acs.accounts.0c00408.

31 S. Chatterjee, S. N. Kramer, B. Wellnitz, A. Kim and L. Kisley, Spatially resolving size effects on diffusivity in nanoporous extracellular matrix-like materials with fluorescence correlation spectroscopy super-resolution optical fluctuation imaging, *J. Phys. Chem. B*, 2023, **127**(20), 4430–4440. Available from: https://pubs.acs.org/doi/full/10.1021/acs.jpcb.3c00941.

32 S. Yoshida, S. Yoshida, W. Schmid, W. Schmid, W. Schmid and N. Vo, *et al.*, Computationally-efficient spatiotemporal correla-tion analysis super-resolves anomalous diffusion, *Opt. Express*, 2021, **29**(5), 7616–7629. Available from: https://opg.optica.org/viewmedia.cfm?uri=oe-29-5-7616&seq=0&html=true.

33 S. Yoshida and L. Kisley, Super-resolution fluorescence imaging of extracellular environments, *Spectrochim. Acta, Part A*, 2021, **257**, 119767.

34 J. Antarasen, B. Wellnitz, S. N. Kramer, S. Chatterjee and L. Kisley, Cross-correlation increases sampling in diffusion-based super-resolution optical fluctuation imaging, *Chem. Biomed. Imaging*, 2024, **2**(9), 640–650, Available from: https://pubs.acs.org/doi/10.1021/cbmi.4c00032.

35 S. N. Kramer, J. Antarasen, C. R. Reinholt and L. Kisley, A practical guide to light-sheet microscopy for nanoscale ima-ging: Looking beyond the cell, *J. Appl. Phys.*, 2024, **136**(9), 091101. Available from: https://pubs.aip.org/jap/article/136/9/091101/3311159/A-practical-guide-to-light-sheet-microscopy-for.

36 L. Kisley, R. Brunetti, L. J. Tauzin, B. Shuang, X. Yi and A. W. Kirkeminde, *et al.*, Characterization of porous materials by fluorescence correlation spectroscopy super-resolution optical fluctuation imaging, *ACS Nano*, 2015, **9**(9), 9158–9166. Available from: https://pubs.acs.org/doi/10.1021/acsnano.5b03430.

37 K. A. Rosowski, T. Sai, E. Vidal-Henriquez, D. Zwicker, R. W. Style and E. R. Dufresne, Elastic ripening and inhibition of liquid–liquid phase separation, *Nat. Phys.*, 2020, **16**(4),

422–425. Available from: https://www.nature.com/articles/s41567-019-0767-2.

38 R. W. Style, T. Sai, N. Fanelli, M. Ijavi, K. Smith-Mannschott and Q. Xu, *et al.*, Liquid-liquid phase separation in an elastic network, *Phys. Rev. X*, 2018, **8**(1), 11028.

39 Y. Shin and C. P. Brangwynne, Liquid phase condensation in cell physiology and disease, *Science*, 2017, **357**(635), 1253.

40 A. A. Hyman, C. A. Weber and F. Jülicher, Liquid-liquid phase separation in biology, *Annu. Rev. Cell Dev. Biol.*, 2014, **30**, 39–58.

41 F. Gobeaux, G. Mosser, A. Anglo, P. Panine, P. Davidson and M.-M. Giraud-Guille, *et al.*, Fibrillogenesis in dense collagen solutions: A physicochemical study, *J. Mol. Biol.*, 2008, **376**(5), 1509–1522. Available from: https://linkinghub.elsevier.com/retrieve/pii/S0022283607016762.

42 K. G. Wilcox, K. R. Yamagami, B. K. Roopnarine, A. Linscott and S. Morozova, Effect of polymer gel elasticity on complex coacervate phase behavior, *ACS Polym. Au*, 2023, **4**(2), 109–119, Available from: https://pubs.acs.org/doi/full/10.1021/acspolymersau.3c00027.

43 EPC Elastin Products Company > Collagens > CN276, COLLAGEN, TYPE II, From bovine nasal. Available from: https://www.elastin.com/product/cn276-collagen-type-ii-from-bovine-nasal.

44 G. D. Pins, D. L. Christiansen, R. Patel and F. H. Silver, Self-assembly of collagen fibers. influence of fibrillar alignment and decorin on mechanical properties, *Biophys. J.*, 1997, **73**, 2164–2172.

45 S. Sheth, E. Jain, A. Karadaghy, S. Syed, H. Stevenson and S. P. Zustiak, UV dose governs uv-polymerized polyacrylamide hydrogel modulus, *Int. J. Polym. Sci.*, 2017, **2017**, DOI: 10.1155/2017/5147482.

46 S. M. Siadat, A. A. Silverman, M. E. Susilo, J. A. Paten, C. A. DiMarzio and J. W. Ruberti, Development of fluorescently labeled, functional type i collagen molecules, *Macromol. Biosci.*, 2022, **22**(3), 2100144. Available from: https://onlinelibrary.wiley.com/doi/full/10.1002/mabi.202100144.

47 F. Nudelman, G. de With and N. A. J. M. Sommerdijk, Cryo-electron tomography: 3-dimensional imaging of soft matter, *Soft Matter*, 2011, **7**(1), 17–24. Available from: https://xlink.rsc.org/?DOI=C0SM00441C.

48 A. Saini, H. Messenger and L. Kisley, Fluorophores "turned-On" by corrosion reactions can be detected at the single-molecule level, *ACS Appl. Mater. Interfaces*, 2021, **13**(1), 2000–2006. Available from: https://pubs.acs.org/doi/abs/10.1021/acsami.0c18994.

49 M. Tokunaga, N. Imamoto and K. Sakata-Sogawa, Highly inclined thin illumination enables clear single-molecule imaging in cells, *Nat. Methods*, 2008, **5**(2), 159–161. Available from: https://www.nature.com/articles/nmeth1171.

50 R. Monge Neria and L. Kisley, Single-molecule imaging in commercial stationary phase particles using highly inclined

and laminated optical sheet microscopy, *Anal. Chem.*, 2023, **95**(4), 2245–2252. Available from: https://pubs.acs.org/doi/abs/10.1021/acs.analchem.2c03753.

51 F. Ortolani, M. Giordano and M. Marchini, A Model for type ii collagen fibrils: distinctive d-band patterns in native and reconstituted fibrils compared with sequence data for helix and telopeptide domains, *Biopolym.: Orig. Res. Biomol.*, 2000, **54**, 448–463.

52 S. Yamaguchi, E. Yamamoto, T. Mannen, T. Nagamune, T. Koudelakova and S. Bidmanova, *et al.*, Nanoscale structure of type I collagen fibrils: Quantitative measurement of D-spacing, *Biotechnol. J.*, 2013, **8**(1), 117–126. Available from: https://onlinelibrary.wiley.com/doi/full/10.1002/biot.201200174.

53 L.-A. DiCecco, R. Gao, J. L. Gray, D. F. Kelly, E. D. Sone and K. Grandfield, Liquid transmission electron microscopy for probing collagen biomineralization, *Nano Lett.*, 2023, **23**(21), 9760–9768. Available from: https://pubs.acs.org/doi/10.1021/acs.nanolett.3c02344.

54 D. A. Cisneros, C. Hung, C. M. Franz and D. J. Muller, Observing growth steps of collagen self-assembly by time-lapse high-resolution atomic force microscopy, *J. Struct. Biol.*, 2006, **154**(3), 232–245. Available from: https://linkinghub.elsevier.com/retrieve/pii/S1047847706000529.

55 S. Morozova and M. Muthukumar, Electrostatic effects in collagen fibril formation, *J. Chem. Phys.*, 2018, **149**(16), 163333.

56 M. Rubinstein and R. H. Colby, *Polymer Physics*, Oxford University Press, 2003, Available from: https://books.google.com/books/about/Polymer_Physics.html?id=RHksknEQYsYC.

57 T. Bhattacharjee and S. S. Datta, Bacterial hopping and trapping in porous media, *Nat. Commun.*, 2019, **10**(1), 1–9. Available from: https://www.nature.com/articles/s41467-019-10115-1.

58 C. Xue, Y. Huang, X. Zheng and G. Hu, Hopping behavior mediates the anomalous confined diffusion of nanoparticles in porous hydrogels, *J. Phys. Chem. Lett.*, 2022, **13**(45), 10612–10620. Available from: https://pubs.acs.org/doi/10.1021/acs.jpclett.2c02733.

59 V. Sorichetti, V. Hugouvieux and W. Kob, Dynamics of nanoparticles in polydisperse polymer networks: from free diffusion to hopping, *Macromolecules*, 2021, **54**(18), 8575–8589. Available from: https://pubs.acs.org/doi/abs/10.1021/acs.macromol.1c01394.

60 B. Mei, T. W. Lin, G. S. Sheridan, C. M. Evans, C. E. Sing and K. S. Schweizer, How segmental dynamics and mesh confinement determine the selective diffusivity of molecules in cross-linked dense polymer networks, *ACS Cent. Sci.*, 2023, **9**(3), 508–518. Available from: https://pubs.acs.org/doi/full/10.1021/acscentsci.2c01373.